

Subaru Deep Spectroscopy of the Very Extended Emission-Line Region of NGC 4388: Ram Pressure Stripped Gas Ionized by the Nuclear Radiation ¹

Michitoshi Yoshida^{2,3}, Youichi Ohyama⁴, Masanori Iye², Kentaro Aoki⁴, Nobunari Kashikawa², Toshiyuki Sasaki⁴, Kazuhiro Shimasaku⁵, Masafumi Yagi², Sadanori Okamura⁵, Mamoru Doi⁶, Hisanori Furusawa^{4,5}, Masaru Hamabe⁷, Masahiko Kimura⁸, Yutaka Komiyama⁴, Masayuki Miyazaki⁵, Satoshi Miyazaki⁴, Fumiaki Nakata⁵, Masami Ouchi⁵, Maki Sekiguchi⁹ AND Naoki Yasuda¹⁰,

ABSTRACT

We report here the results of deep optical spectroscopy of the very extended emission-line region (VEELR) found serendipitously around the Seyfert 2 galaxy NGC 4388 in the Virgo cluster using the Subaru Telescope. The H α recession velocities of most of the filaments of the region observed are highly blue-shifted with respect to the systemic velocity of the galaxy. The velocity field is complicated, and from the kinematic and morphological points of view, there seem to be several streams of filaments: low velocity filaments, with radial velocities v with respect to the systemic velocity of NGC 4388 ~ -100 km s⁻¹, high velocity ($v \sim -300$ km s⁻¹) filaments, and a very high velocity ($v \sim -500$ km s⁻¹) cloud complex. The emission-line ratios of the VEELR filaments are well explained by power-law photoionization models with solar abundances, suggesting that the Seyfert nucleus of NGC 4388 is the dominant ionization source of the VEELR and that the VEELR gas has moderate metallicity. In addition to photoionization, shock heating probably contributes to the ionization of the gas. In particular, the filaments outside the ionization cone of the Seyfert nucleus are mainly excited by shocks. The predicted shock velocity is $\sim 200 - 300$ km s⁻¹, which is comparable to the velocities of the filaments. We conclude that the VEELR was formerly the disk gas of NGC 4388, which has been stripped by ram pressure due to the interaction between the hot intra-cluster medium (ICM) and the galaxy. The velocity field and the morphology of the VEELR closely resemble snapshots from some numerical simulations of this process. In the case of NGC 4388, the ram pressure-stripped gas, which is normally seen as extended H I filaments, happens to be exposed and ionized by the radiation from the AGN, and so can be seen as optical emission-line gas.

Subject headings: galaxies: clusters: general — galaxies: evolution — galaxies: individual (NGC 4388) — galaxies: kinematics and dynamics — galaxies: Seyfert — intergalactic medium

²Optical and Infrared Astronomy Division, National Astronomical Observatory, Mitaka, Tokyo 181-8588, Japan.

³Okayama Astrophysical Observatory, National Astronomical Observatory, Kamogata, Okayama 719-0232, Japan; yoshida@oao.nao.ac.jp.

⁴Subaru Telescope, National Astronomical Observatory of Japan, 650 North A'Ohoku Place, Hilo, HI 96720, USA.

⁵Department of Astronomy, University of Tokyo, Tokyo 113-0033, Japan.

⁶Institute of Astronomy, University of Tokyo, Mitaka,

Tokyo 181-8588, Japan.

⁷Department of Mathematical and Physical Sciences, Japan Women's University, Bunkyo-ku, Tokyo 112-8681, Japan.

⁸Department of Astronomy, Kyoto University, Kyoto 606-8502, Japan.

⁹Institute for Cosmic Ray Research, University of Tokyo, Kashiwa, Chiba 277-8582, Japan.

¹⁰Astronomical Data Analysis Center, National Astro-

1. INTRODUCTION

Determination of the environmental effects on the evolution of galaxies has been one of the main subjects of extragalactic astronomy. It is widely believed that phenomena such as morphology segregation and color evolution of galaxies in clusters of galaxies provide important clues to the nature of these environmental effects.

Morphology segregation of galaxies in clusters has been well known since the 1970s (Oemler 1974; Melnick and Sargent 1977), — early-type galaxies are the dominant population at the central region of a cluster, while late-type galaxies are preferentially distributed at the outskirts. Dressler (1980) found a good correlation between galaxy morphology and the number density of galaxies in the local universe and generalized the morphology segregation of cluster galaxies in terms of a density – morphology relationship. Postman and Geller (1984) found that this relationship extends over six orders of magnitude in galaxy density.

Meanwhile, Butcher and Oemler (1978, 1984) reported observational evidence of the increase of blue galaxy fraction at high redshift clusters, which is known as the “Butcher-Oemler effect” (Butcher and Oemler 1978, 1984). In addition, recent deep imaging studies of high redshift clusters performed with the *Hubble Space Telescope* have revealed that the majority of the blue galaxy population of high- z clusters consists of star-forming normal late-type disk galaxies (e.g., Dressler et al. 1994, 1997; Couch et al. 1998; Fasano et al. 2000). This population is thought to be made up of field galaxies captured by clusters, in the context of the hierarchical structure formation scenario within a cold dark matter (CDM) cosmology, which is the most successful model of the universe. These findings suggest that galaxies captured by a cluster should change their morphology and color as they fall into the cluster center (Abraham et al. 1996; Oemler, Dressler & Butcher 1997; Poggianti et al. 1999).

Several mechanisms for driving the morphology and color evolution of galaxies in clusters of galaxies have been proposed. These include succes-

sive fast, shallow encounters of galaxies (“galaxy harassment”) (Moore et al. 1996; Moore et al. 1998); close galaxy – galaxy interactions, such as mergers (Walker, Mihos, & Hernquist 1996; Kauffmann & Charlot 1998; Okamoto & Nagashima 2001); removal of the halo gas by interactions with the hot intra-cluster medium (ICM) (Larson, Tinsley & Caldwell 1980; Bekki, Couch & Shioya 2002); or ram pressure stripping of the disk gas by the hot ICM (Abadi et al. 1999; Quilis, Moore & Bower 2000; Vollmer, Cayatte, Balkowski, & Duschl 2001 (hereafter referred to as VCBG); Schulz and Struck 2001 (hereafter referred to as SS01)). It is still not clear which of these mechanisms plays the greatest role in the evolution of cluster galaxies, although there have been many observational and theoretical studies. Nevertheless, it is clear that the rapid and drastic consumption of the interstellar matter of a galaxy as it passes through a cluster is the key to its evolution. Thus, detailed observational studies of the sites at which violent gas consumption is occurring, such as large-scale outflows or strong starbursts, would help us to understand this problem.

Recently, Yoshida et al. (2002; hereafter referred to as YOS02) found a very large region of ionized gas extending around a Seyfert 2 galaxy in the Virgo cluster, NGC 4388. This very extended emission-line region (the “VEELR”) has a size of ≈ 35 kpc and is located preferentially toward the northeastern side of the galaxy. The region consists of many filaments or clouds, with a typical size of ~ 100 pc. The total ionized gas mass of the VEELR is $\sim 10^5 M_{\odot}$. The $[\text{O III}]\lambda 5007/\text{H}\alpha$ emission-line intensity ratios of the filaments, and the observation that the ratios decrease monotonically with distance from the galactic center, suggest that the primary ionization source of the region may be the Seyfert nucleus of NGC 4388. YOS02 proposed two possible hypotheses concerning the origin of the VEELR gas: it may be either (1) the tidal debris of a past minor merger or (2) the ram pressure-stripped gas due to the collision between the galaxy and the intra-cluster medium (ICM) of the Virgo cluster. In either case, such a large gas flow outside the galaxy disk must be closely related to the evolution of NGC 4388 and the surrounding ICM, and thus detailed investigation of the VEELR should provide important clues regarding the evolution of galaxies and the ICM in

nomical Observatory, Mitaka, Tokyo 181-8588, Japan.

¹Based on data collected at the Subaru Telescope, which is operated by the National Astronomical Observatory of Japan.

clusters of galaxies.

To determine the nature and origin of the VEELR in NGC 4388 in detail, we have carried out deep optical spectroscopic observations of the VEELR filaments using the Subaru Telescope. We adopted a distance of 16.7 Mpc to NGC 4388 (Yasuda et al. 1997) throughout this study.

2. OBSERVATIONS

The observations were made with the FOCAS (Faint Object Camera And Spectrograph; Kashikawa et al. 2002) attached at the Cassegrain focus of the Subaru Telescope (Kaifu et al. 2000) on 2002 March 11. We used the multi-slit spectroscopy mode of FOCAS to obtain the spectra of as many of the bright filaments of the VEELR as possible, given their complicated spatial distribution. We used two slit masks, “MOS mask 1” and “MOS mask 2,” and obtained the spectra of 40 filaments or clouds within the 6′ field of view of FOCAS. The PA of the slits of MOS mask 1 was 145° , and that of MOS mask 2 was -55° . The layouts of the slits are shown in Figures 1 and 2.

The width of each slit was $0''.8$ on the sky. We used a grating of 300 grooves/mm: the combination of the grating and the slit width gave a resultant spectral resolving power of ≈ 650 at 6600 \AA . The detector is a mosaic CCD consisting of two $2K \times 4K$ MIT/Lincoln Lab. CCDs. The pixel scale of the CCDs is $0''.1$ / pixel. We binned 3 pixels in the spatial direction and 4 pixels in the wavelength direction on the chip. Each spectrum covers the wavelength range from 4700 \AA to 7500 \AA . We obtained six 1800-s exposures and three 1800-s exposures for MOS mask 1 and MOS mask 2, respectively, to improve the signal-to-noise ratio and to allow us to avoid cosmic ray events and bad pixels of the detector by taking median values in combining the spectra. The total exposure times were therefore 3 hours and 1.5 hours for MOS mask 1 and MOS mask 2, respectively.

Unfortunately, one CCD chip of the mosaic CCD has several defects and bad columns and has a problem in charge transfer around the defects, so that some regions of the CCD are covered by strong spurious patterns. Although the total area of these spurious patterns is rather small as a fraction of the total CCD area — less than 1 % —, some spectra were corrupted by this effect. We

note all spectra that suffer from this problem in Table 1 below.

We observed a spectrophotometric standard star, BD+33 2642, for flux calibration. In observing the standard star we used a slit $2''$ wide. The night was almost completely clear, but some patches of thin clouds occasionally passed in front of the field of view. Seeing during the observing night was stable and around $0''.7$.

3. DATA REDUCTION

Data reduction was carried out using a special data reduction package developed within IRAF¹¹ and IDL for FOCAS multi-slit data (Yoshida et al. 2000; Kashikawa et al. 2002). After the bias levels, which were estimated using the over-scan regions of the CCD chips, were subtracted from each frame, flat fielding was performed using the dome flat data. The field distortion of FOCAS was corrected simultaneously with the flat-fielding.

We used the night-sky emission lines as wavelength calibration data for $\lambda > 5700 \text{ \AA}$, and Thorium arc line data at shorter wavelengths. The wavelength calibration was accurate enough to investigate the kinematics of the VEELR gas near the $H\alpha$ line; the r.m.s. calibration error for $\lambda > 5500 \text{ \AA}$ is $\approx 0.2 \text{ \AA}$, corresponding to 10 km s^{-1} in radial velocity at $\lambda = 6000 \text{ \AA}$. The accuracy of absolute wavelength calibration for the shortward wavelengths, i.e., $\lambda < 5500 \text{ \AA}$, was worse than for the red region; the calibration error is about 1 \AA r.m.s., because the arc line data were obtained several times during the observation and the positions of the spectra on the CCDs are slightly shifted due to flexure of the FOCAS instrument between the object exposure and the arc line exposure. Hence, we used only $H\alpha$ data to measure radial velocities.

After subtracting sky emission from the data, we carried out flux calibration using the standard star data and the standard extinction curve at Mauna Kea. The flux calibration error, which was estimated from the variation of the resultant fluxes of the calibrated spectra of different frames, was sometimes as high as 30 %. Most of this inaccuracy was caused by the unstable sky conditions of

¹¹IRAF is distributed by the National Optical Astronomy Observatories, which are operated by the Association of Universities for Research in Astronomy, Inc., under cooperative agreement with the National Science Foundation.

the night of the observations, as mentioned in the previous section. The flux calibrated spectra were rescaled with respect to the frames showing the highest count rate, then combined by taking the median value of the frames. We summed the two-dimensional spectrum of each slit along the direction of the slit length and made a one-dimensional spectrum. The integration lengths along the slits are listed in column 3 of Table 1 in units of parsec. In some slits, there are at least two spatially separated gas components, which differ from each other both in kinematics or and in excitation. We extracted such components separately from the two-dimensional spectrum if they were present. Such components are indicated by adding the suffixes “-1,” “-2,” etc. to the slit IDs in Table 1. For example, the spectrum of the slit M1-17 has two components with relative velocities of -145 km s^{-1} and -438 km s^{-1} , respectively: these are denoted “M1-17-1” and “M1-17-2,” respectively.

The emission-line characteristics (FWHMs, central wavelengths, and intensities) were measured by fitting Gaussian functions. We fitted the $\text{H}\alpha$ and $[\text{N II}] \lambda\lambda 6548, 6584$ doublet simultaneously, assuming the same recession velocity and velocity dispersion for the three emission-lines and a fixed emission-line intensity ratio of 3.0 for $[\text{N II}] \lambda 6584/[\text{N II}] \lambda 6548$. We fitted the $[\text{S II}] \lambda\lambda 6717, 6731$ doublet assuming the same recession velocity and velocity dispersion for the two lines. We made the same assumption with a fixed line intensity ratio of 3.0, for $[\text{O III}] \lambda 5007/[\text{O III}] \lambda 4959$ in fitting $\text{H}\beta$ and $[\text{O III}] \lambda\lambda 4959, 5007$ doublet. Unfortunately, the $[\text{O I}] \lambda 6300$ emission-line of the object falls near a bright sky emission-line of $[\text{O I}] \lambda 6364$. The intrinsic weakness of the $[\text{O I}]$ line, coupled with this problem, prevented us from measuring the $[\text{O I}]$ emission-line parameters accurately, except in rather bright cases.

4. RESULTS

The physical parameters of the VEELR filaments are tabulated in Table 1. The recession velocities of the filaments shown in column 5 are those of $\text{H}\alpha$. As the spectral resolution of our spectra, ~ 650 , is too low to allow accurate measurement of the velocity dispersion of the emission-lines, we list the values for clearly resolved, high signal-to-noise data in column 6.

Instrumental broadening of the emission line was roughly corrected using the following simple equation: $\sigma_{true} = (\sigma_{obs}^2 - \sigma_{ins}^2)^{1/2}$, where σ_{obs} is the observed emission-line width and σ_{ins} is the instrumental line width. Column 7 of Table 1 shows the names of individual clouds as given by YOS02.

The electron densities N_e were obtained from the intensity ratios of $[\text{S II}] \lambda 6717/[\text{S II}] \lambda 6731$ under the assumption that the ionized gas temperature is 10^4 K (Osterbrock 1989). We found that the $[\text{S II}] \lambda 6731$ lines of most filaments of the VEELR are too weak, relative to the $[\text{S II}] \lambda 6717$ line, to allow accurate determination of N_e : that is, the N_e s of the VEELR filaments are lower than $\sim 50 \text{ cm}^{-3}$.

The emission-line intensity ratios of $[\text{O III}] \lambda 5007/\text{H}\beta$, $[\text{N II}] \lambda 6584/\text{H}\alpha$, $[\text{S II}] \lambda 6717 + \lambda 6731/\text{H}\alpha$ and $[\text{O I}] \lambda 6300/\text{H}\alpha$ are summarized in Table 2.

4.1. Velocity field

The velocity field of the VEELR is shown in Figure 3. The velocities of almost all the filaments measured are blue-shifted relative to the systemic velocity of the galaxy. The velocities show a very wide range ($\sim 700 \text{ km s}^{-1}$) from $\sim -50 \text{ km s}^{-1}$ to over -700 km s^{-1} .

The overall velocity field of the VEELR is quite complicated and could be dominated by significant turbulent motion. There is no smooth velocity gradient across the region. Although we measured only a fraction of the filaments in the region, several kinematic groups seem to be represented (see Figure 4).

First, a string of relatively low velocity, $\sim -50 \text{ km s}^{-1} - -200 \text{ km s}^{-1}$, filaments (hereafter referred to as the “LV filaments”) was found along a line originating at around PA 65° and $r \approx 175''$ (14.2 kpc; M2-10) northeast from the nucleus and extended along PA 55° .

Second, a group of high velocity, $\sim -200 \text{ km s}^{-1} - -450 \text{ km s}^{-1}$, filaments (hereafter referred to as the “HV filaments”) are distributed over the region. The HV filaments can be broken down into the following three groups: the “NE-HV filaments,” the “N-HV filaments,” and the “W-HV filaments.” The NE-HV filaments are a bow-like string of filaments that extend from the cloud at PA 65° , $r \approx 290''$ (around M2-14) to the north along PA 10° . The N-HV filaments are a group

of clouds at PA 40° , $r \approx 110''$ (around M1-5 and M2-6), PA 32° , $r \approx 170''$ (M1-9 and M1-10) and PA 45° , $r \approx 195''$ (M1-11 and M2-11). The W-HV filaments consist of a bright, dumbbell-like cloud, corresponding to the “C26” of YOS02, located at PA 95° and $r \approx 125''$ (M1-1, M1-2 and M2-5), and a bright cloud at PA 70° and $r \approx 155''$ (M2-9), corresponding to “C25” of YOS02.

Third, there is a group of very high velocity clouds/filaments (hereafter referred to as the “VHV clouds”) around the region where PA = 40° , $r \approx 145''$ (M1-7, M1-8, M2-7 and M2-8). The typical radial velocity of the VHV clouds is ~ -550 km s $^{-1}$, and one of these clouds even has a velocity of ~ -750 km s $^{-1}$. The VHV clouds are embedded in a string of filaments that extend from PA 50° , $r \approx 70''$ toward the north-northeast (PA 15°). This string of filaments contains the N-HV filaments and the VHV clouds. The morphology of this string suggests that the VHV clouds are part of one stream. If this were the case, the high velocity motion of the VHV clouds could be interpreted as a projection effect of the helical motion of an outflow stream. However, the helical motion velocity of the stream would then reach up to 200 km s $^{-1}$, which is too fast to maintain the shape of the stream unless there is a very strong confinement force, such as a strong magnetic field. Thus, the greater fraction of their high velocities cannot be interpreted as a projection of a helical motion of the stream. Instead, the VHV clouds must be accelerated radially by some as yet undetermined mechanism.

These names for the groups (the “LV filaments,” “NE-HV filaments,” “N-HV filaments,” “W-HV filaments,” and “VHV clouds”) are given in column 8 of Table 1. In addition, the spectra of the NE plume¹² and the galaxy disk are labeled as “NEp” and “disk” in column 8 of Table 1.

The positions and possible extensions of these filament/cloud groups are overlaid on the velocity field of the VEELR in Figure 4. Figure 5 shows a position – velocity diagram for the VEELR. The horizontal axis of this diagram represents the dis-

tance from the nucleus in units of kpc. Data points for different filaments/clouds groups are shown as different symbols in this diagram (Figure 5). The groups of filaments mentioned above can be seen to be well separated in position – velocity space.

4.2. Excitation of the filaments

The emission-line spectra of the VEELR filaments are characterized by forbidden line enhancement and are very different from those of extragalactic H II regions. Figure 6 shows some examples of the spectra and Figures 7–9 show diagnostic diagrams for optical emission-lines (Veilleux & Osterbrock 1987). Two different ionization model loci are over-plotted in Figures 7–9. The dotted lines represent a power-law photoionization model calculated with the photoionization code CLOUDY (CLOUDY 94.00: Ferland 1996). We used a simple power-law continuum with a spectral index α of -1.4 as the incident light, assuming a plane parallel cloud geometry with an electron density N_e of 30 cm $^{-3}$ and solar metal abundance. The dotted-dashed lines are the loci of the shock ionization model of Dopita and Sutherland (1995). The loci shown here are for a shock only model with no pre-existing magnetic field.

Figures 7–9 show that the emission-line ratios of almost all the filaments are consistent with a power-law photoionization model with solar metal abundance, suggesting that the filaments have approximately solar abundance and are ionized by the power-law ionizing continuum emerging from the nucleus of NGC 4388. This result is consistent with the conclusions regarding the ionization mechanism of the VEELR reported in previous studies (YOS02; Ciroi et al. 2003). The ionization parameter U , which is the ratio of the number density of ionizing photons to that of electrons, of a typical filament of the VEELR was estimated to be of the order of 10^{-3} from the diagrams (Figure 7–9). The filaments showing relatively high U ($\sim 10^{-2.5}$ – 10^{-3}) tend to be distributed near the nucleus (i.e NE-plume and inner N-HV filaments), whereas low U ($\sim 10^{-3}$ – $10^{-3.5}$) filaments are located far from the nucleus (outer N-HV filaments and VHV filaments). This also supports the AGN photoionization hypothesis.

Some filaments show low excitation spectra. Low excitation emission-lines, such as [O I] and [S II], are enhanced in the spectra of the W-HV

¹²The “NE plume” is the bright extra-planar emission-line region extending up to ~ 5 kpc to the northeast of the galaxy (e.g., Pogge 1988; Colina 1992; Petitjean and Durret 1993; Veilleux et al. 1999a). The configuration of the extra-planar emission-line region of NGC 4388 was illustrated in Figure 2 of YOS02.

filaments (“C26”). On the other hand, [O III] is relatively weak ($[\text{O III}]/\text{H}\beta \sim 1$) in these filaments, in contrast to other high excitation filaments. The emission-lines of the W-HV filaments are also considerably broad (see the bottom right panel of Figure 6). The data points for these regions are distributed around the model locus of the shock model of Dopita and Sutherland (1995) with a shock velocity of $200 - 300 \text{ km s}^{-1}$. These findings strongly suggest that the W-HV filaments are excited by shocks. The W-HV filaments exist outside the ionization cone of the NGC 4388 nucleus (Falcke, Wilson, and Simpson 1998; Veilleux et al. 1999a, YOS02). YOS02 remarked that the excitation mechanism of these “out of the cone” filaments is a mystery, pointing out that there is no counterpart to C26 in the broad-band images (V and R_C images), so that it is not plausible that this filament is a bright H II region at the outskirts of the galaxy disk.

Shock may also contribute to the excitation of the other filaments. Figure 10 shows the $[\text{N II}]/\text{H}\alpha$ ratios of the VEELR filaments as a function of velocity. This figure clearly shows that the [N II] line is enhanced in the VHV clouds (see also the upper right panel of Figure 6). This velocity – excitation coupling indicates that shocks, induced by the rapid motion, can also play a role in excitation of the filaments.

Ciroi et al. (2003) carried out a detailed analysis of the ionization of the VEELR and the SW cone (Falcke, Wilson & Simpson 1998; YOS02) using a composite model of photoionization and shock heating. They used the photometric data of YOS02 for analysis of the VEELR. The ionization parameters they obtained for the VEELR filaments were distributed in the range $10^{-3} - 10^{-5}$. These values are consistent with our results, although they are slightly lower. This subtle discrepancy may be attributed to the contribution of shock heating to ionization of the filaments. Ciroi et al. (2003) suggested that shock heating gives rise to the ionization of the filaments, and derived shock velocities in the range $\sim 30 - 150 \text{ km s}^{-1}$. Note that these values are almost consistent with the shock velocities suggested in the present study for the low excitation clouds of the VEELR.

5. DISCUSSION

5.1. The origin of the VEELR gas

YOS02 discussed the origin of the gas of the VEELR from a morphological point of view, and concluded that there are two possibilities for the origin of the VEELR: it is either the tidal debris of a past minor merger, or the disk gas of NGC 4388 stripped by the ram pressure of the hot ICM. Here, we examine these two scenarios using our new observational results, and discuss the origin of the VEELR gas.

5.1.1. *Minor merger tidal debris hypothesis*

As suggested in YOS02, NGC 4388 might have experienced at least one minor merger in the past. A minor merger affects the dynamics of the primary galaxy and leaves some imprints on its morphology (Hernquist & Mihos 1995; Mihos et al. 1995). Peculiar morphological characteristics of NGC 4388, such as its boxy bulge and central bar, and the faint hump and tail that extend outside the disk, could have formed as a result of the dynamic disturbance induced by a minor merger (YOS02). If the VEELR were the tidal debris of a merger of a gas-rich dwarf galaxy and NGC 4388, the gas in the dwarf should have been stripped by the tidal force of NGC 4388 and the stripped gas would have been left near the path of the dwarf’s fall. If this were the case, the velocity of the VEELR gas relative to NGC 4388 should not exceed the infall velocity of the merging dwarf. However, the measured velocities of the VEELR filaments are $-300 - -400 \text{ km s}^{-1}$, and some filaments show much higher radial velocities, up to -700 km s^{-1} . These velocities are well beyond the escape velocity of NGC 4388 ($\sim \sqrt{2} \times v_{\text{rot}} \approx 250 \text{ km s}^{-1}$, where v_{rot} is taken to be 180 km s^{-1} , following Veilleux et al. 1999b) and so are too high to apply the tidal debris scenario.

In addition, the turbulent nature of the velocity field of the VEELR is not consistent with the minor merger hypothesis. The tidal tails found in and around merging galaxies have smooth velocity fields and mild velocity gradients of the order of $1 - 10 \text{ km s}^{-1} \text{ kpc}^{-1}$ in general (e.g., Smith 1994; Hibberd et al. 1994; Hibberd and Yun 1999). For example, the Magellanic Stream, the nearest example of tidal debris, has a velocity gradient of

$\sim 300 \text{ km s}^{-1}$ over a few tens of kpc (Mathewson, Cleary & Murray 1974). The velocity field of the Magellanic Stream is also smooth and its kpc-scale velocity dispersion does not exceed $\sim 100 \text{ km s}^{-1}$. On the other hand, the VEELR is highly turbulent (see Figures 3, 4). The velocities of the filaments range over 700 km s^{-1} and abrupt velocity changes, with magnitudes of up to $\sim 300 \text{ km s}^{-1}$, are seen over the region.

Further, the emission-line spectra of the VEELR filaments suggest that the metallicity of the VEELR gas is almost at the solar value: there is no evidence that the gas is metal-poor. This is inconsistent with the hypothesis that the VEELR gas was dragged out of a merged gas-rich dwarf galaxy, because a typical gas-rich dwarf galaxy has a metal abundance of 1/10 solar (cf. Vílchez & Iglesias-Páramo 2003).

These results seem to disfavor the minor merger hypothesis. As mentioned above, NGC 4388 might have experienced a minor merger in the past (cf. YOS02), which may have given rise to part of the VEELR. However, it is difficult to explain most of the spectroscopic properties of the VEELR gas only with the minor merger hypothesis. Therefore, we concluded that it is unlikely that the majority of the VEELR gas is tidal debris from a past minor merger.

5.1.2. *Ram pressure stripping hypothesis*

The characteristics of the VEELR described above can be naturally explained by the ram pressure stripping hypothesis.

As noted in YOS02, the morphology of the VEELR strongly resembles some snapshots from the inclined collision models of ram pressure stripping simulations conducted by Abadi et al. (1999), Quilis et al. (2000), VCBDB, and SS01. The one-sided elongation of the VEELR suggests that NGC 4388 has a large transverse velocity toward the southwest. The $\text{H}\alpha$ gas of the inner disk of the galaxy is abruptly truncated at a distance of 5 kpc from the nucleus on the western side, while on the eastern side of the galaxy faint ionized gas extends to the outside of the stellar disk (Figure 1a of YOS02). The H I gas distribution is also asymmetric in the same manner as the $\text{H}\alpha$ gas (Cayatte et al. 1990). This peculiar gas distribution supports the hypothesis that the galaxy is

moving in a southwesterly direction with a large transverse velocity and the disk gas is blown out by ram pressure induced by this galactic motion.

The velocity field of the VEELR can also be interpreted in the context of the ram pressure stripping scenario. While the recession velocity of NGC 4388 is approximately 1500 km s^{-1} larger than the systemic velocity of the Virgo cluster, the galaxy is thought to be located at the vicinity of the cluster core. Thus, NGC 4388 is moving in the Virgo cluster ICM with a line-of-sight velocity of $\approx 1500 \text{ km s}^{-1}$ relative to the ICM. Hence, the blue-shifted velocity field of the VEELR can be explained naturally: the collision between the galaxy and the hot ICM strips the disk gas and the gas is blown in the direction opposite to the motion of the galaxy. Assuming that the direction of the extension of ram pressure-stripped gas is almost the same as the direction of the ICM wind — in other words, the stripped gas is blown along the wind direction — and that the inclination angle of the VEELR with respect to our line of sight is 45° , the transverse velocity is also $\sim 1500 \text{ km s}^{-1}$ and the total infalling velocity of NGC 4388 toward the Virgo cluster center reaches $\sim 2300 \text{ km s}^{-1}$.

Turbulent nature of the velocity field of the VEELR can also be explained by high speed collision between the galaxy and the hot ICM. Strong ram pressure from the ICM should induce turbulent motion in the stripped gas stream.

As described above, there seem to be a number of groups of kinematically related filaments in the VEELR: the LV filaments, the HV filaments, and the VHV clouds. VCBDB presented some results of a series of numerical simulations based on inclined collision models of ram pressure stripping. Edge-on snapshots of a model of VCBDB with an inclination angle of 45° and a colliding velocity of $\sim 1000 \text{ km s}^{-1}$ show that the disk gas of the primary galaxy forms two streams as it is stripped. One of the streams begins at the disk edge at the nearside of the ICM wind and the other at the far side of the wind. The latter stream is removed from the disk more rapidly than the former. Thus, it is suggested that the LV filaments correspond to the former stream, while the HV and VHV clouds are embedded in the latter.

In addition, ram pressure stripping scenario has no problem in explaining high metallicity of

the VEELR gas. It is natural for the extended gas to have the same metallicity, approximately Solar value, to the galaxy disk, if the gas is stripped from the galaxy by ram pressure.

Therefore, the new spectroscopic data presented here led us to the conclusion that it is most likely that the VEELR gas is the disk gas of NGC 4388 stripped by the ram pressure of the hot ICM. A spatial coincidence between the VEELR and the soft X-ray gas around NGC 4388, which was found recently by detailed analysis of *Chandra* archival data (Iizuka, Kunieda & Maeda 2003) also supports the ram pressure stripping hypothesis. If this is the case, we have detected ram pressure-stripped gas in the form of warm ($T \sim 10^4$ K) ionized gas (the VEELR) very far away from a cluster galaxy. The ionization of the stripped gas by a powerful AGN, together with the deep imaging capability of an 8-m class telescope, have made it possible to detect this faint structure.

Although there have been many observational studies of ram pressure stripping phenomena (e.g., Cayatte et al. 1990; Gavazzi et al. 1995; Phookun & Mundy 1995; Ryder et al. 1997; Kenney & Koopmann 1999; Vollmer et al. 2000; Vollmer, Braine et al. 2001; Bureau & Carignan 2002), the present study is the first to have revealed the detailed morphology and kinematics of the ram pressure-stripped gas over a few tens of kpc¹³. In fact, the situation of NGC 4388 is rather special, in that the majority of the stripped gas happens to pass into the ionizing radiation cone of the Seyfert nucleus, and as a consequence a part of the stripped gas is ionized and visible as optical emission-line gas. The case of NGC 4388 provides a rare opportunity to investigate the warm phase of ram pressure-stripped gas in detail.

We discuss the VEELR in the context of the ram pressure stripping hypothesis in the following sections.

5.2. The VEELR and intracluster star formation activity

In this section, we briefly discuss the fate of the VEELR gas and examine the possibility of star formation in the VEELR.

The discovery of the VEELR indicates that some part of the ram pressure-stripped gas survives throughout the stripping process and does not evaporate for a significantly long time ($\sim 10^8$ yr)¹⁴. V CBD pointed out that the disk gas of the galaxy would be stripped in the form of an ensemble of relatively dense cloudlets, each of which would be dense enough to prevent its evaporation in the hot ICM during ram pressure stripping. Those cloudlets would survive in the hot ICM for a long time ($t > 10^8$ yr). According to V CBD, the stripped cloudlets would cool radiatively and become denser with time, so that molecules would be formed in their cores.

SS01 also pointed out that the radiative cooling of ram pressure-stripped gas could be important in cases in which the stripped gas density is higher than a critical density, which is determined by the strength of the ram pressure. They estimated that the critical density would be of the order of ~ 1 cm⁻³ for the Virgo cluster (SS01). Although our spectroscopic results did not provide a definite value for the electron densities of the VEELR filaments (they are too low to be derived from [S II] emission line ratios) YOS02 estimated the r.m.s. electron density of each filament to be ~ 0.5 cm⁻³ from H α photometry. Hence, assuming a typical volume filling factor of interstellar ionized gas, $f_v \sim 10^{-3} - 10^{-4}$ (e.g., Robinson et al. 1994), for the VEELR filaments, we estimate the local densities of the line emitting clouds to be ~ 10 cm⁻³. This is high enough to make radiative cooling dominant in the thermal balance of the stripped gas. The filamentary structure of the VEELR also suggests that radiative cooling and thermal instability cause the stripped gas to condense.

In the VEELR, there are a number of filaments that could be ionized by the radiative shock induced by a collision between the disk ISM and

¹³Gavazzi et al. (2001) detected very large (~ 75 kpc) warm ionized gas around the two irregular galaxies in the cluster of galaxies Abell 1367, and concluded that these are ram pressure-stripped material. This material is twice as large as the VEELR of NGC 4388, but its detailed morphology and the kinematics are not known.

¹⁴The size and the radial velocity of the VEELR are ~ 35 kpc and ~ 300 km s⁻¹, respectively. Assuming that the inclination angle of the VEELR is 45°, we estimated the age of the VEELR as $\sim 10^8$ yr

the hot ICM. Although the main ionization source should be the nuclear power-law radiation, shock waves accompanied with rapid motion could be responsible for the ionization of some HV filaments and VHV clouds. In fact, for some VHV clouds that are distant from the nucleus, low ionization emission-lines, such as [N II] or [S II], tend to be enhanced, suggesting that shock heating plays some role in their ionization. Successive shocks would condense the filaments significantly. Therefore, the physical state of the VEELR filaments allows them to form molecules internally, and to eventually form stars.

Recently, Gerhard et al. (2002) found an intergalactic compact star-forming region near NGC 4388. The location of the region is about 20 kpc north of the disk of NGC 4388. Although it is far away from the main stream of the VEELR, it is worth noting that its distance from the galaxy is comparable to that of the extension of the VEELR. This region might be a gas clump that has split off from the main stream of the VEELR. If this is the case, this region is the first known example of star formation within ram pressure-stripped gas.

Our data suggest that ram pressure-stripped gas can survive for a long time after stripping and it might be dense enough to cool radiatively. As mentioned above, stars might be formed in such cool gas. It is, however, no better than a speculation. In order to obtain some conclusive results on intracluster star formation and its relationship with ram pressure-stripping phenomenon, deep observations of neutral gas, H I or CO molecule, would be crucial.

5.3. Comparison with radio observations: interaction of disk star formation with the VEELR

We compared the deep H α and [O III] images of NGC 4388 taken by YOS02 with radio observations to investigate how the active star formation of NGC 4388 affects the extra-planar plasma evolution.

Irwin et al. (1999) conducted VLA 20 cm and 6 cm observations of NGC 4388 as a part of a series of studies of extended radio plasma around edge-on galaxies. They found very extended, faint radio emission on both sides of the disk of the galaxy at

20 cm. The morphology of this emission is peculiar: it has a “cracked” X-shape. It extends in three directions from the disk (to the northwest, southeast, and southwest) but not in the northeasterly direction, which is the direction of extension of the VEELR. The radio images of Irwin et al. are overlaid on the H α image from YOS02 in Figure 11b. We found faint extra-planar spurs in the H α image of NGC 4388 (Figure 11d). The directions of these spurs agree well with the direction of the extended radio emission. On the northeastern side of the galaxy, the bright NE plume and the VEELR prevent the identification of such faint structures.

Irwin et al. (1999) also found, at 6 cm, a striking extension originating on the eastern side of the disk (10'' east of the nucleus) and extending northwards. The size of this extension is comparable to that of the NE-HV filaments, whereas it is located between the complex of the NE-HV filaments and the VHV clouds and the NE plume (see Figure 11c). In other words, the extra-planar radio plasma and the optical emission-line gas seem to be anti-correlated in spatial distribution. This raises the question of the significance of this spatial anti-correlation.

The faint radio emission seen at 20 cm and the northeastern extension detected at 6 cm may be parts of a large X-shaped, starburst-driven superwind (Chevalier & Clegg 1985; Heckman, Armus & Miley, 1990; Strickland & Stevens 2000) from the disk of NGC 4388. To the northeastern side of the outflow, the radio-emitting plasma may be accelerated by the turbulent motion of the ram pressure-stripped ionized gas through some particle acceleration mechanisms such as Fermi acceleration or shock acceleration (cf. Webb et al. 2003; references are therein). The spatial anti-correlation between the emission-line gas and the radio-emitting plasma suggests an interaction between the two components. This effect might change the energy distribution of the radio-emitting plasma toward high energy, causing the spectral index of the northeast extension to become harder than the other wind plasma. Thus, the counterpart of the northeast extension may be lost in the low energy band (i.e., 20 cm).

The interaction between the VEELR gas and the starburst superwind may also accelerate the VEELR gas. The VHV clouds are located just

outside of the northeast top of the 6-cm radio emission. This spatial coincidence supports the above suggestion. In other words, parts of the NE-HV filaments may be accelerated by the superwind and form the VHV clouds. This interaction would induce shock-waves in the VHV clouds and the shocks would excite the gas. The shock-like excitation property of the VHV clouds which was mentioned in section 4.2 is naturally explained by this scenario.

An extended X-shaped structure has also been found in soft X-ray emission. The *ROSAT* HRI image of NGC 4388, reduced by Colbert et al. (1998), shows an X-shaped structure. Although the scale of this emission is considerably smaller than the radio emission, the position angles of the legs of the “X”s are in good agreement. The size and the luminosity of the HRI emission is comparable to those of the HRI emissions of the starburst galaxy NGC 2146 (Armus et al. 1995). Recently, the extra-planar soft X-ray emission is found to be more extended toward the south of the galaxy at very faint level by a deep X-ray image of NGC 4388 taken by *Chandra* (Iizuka, Kunieda, & Maeda 2003). As mentioned in section 5.1.2., the largest component of this faint X-ray emission is extended toward the north-eastern direction, which is attributed to the ram pressure stripping. The southern extension of this faint X-ray emission is seen like an extension of the central “X” shaped X-ray emission of *ROSAT*. These X-ray characteristics also suggest that a superwind blows from the NGC 4388 disk and interacts with the VEELR or the hot ICM wind.

The disk radio emission of NGC 4388 should be a result of active star-forming regions in the galaxy disk¹⁵. SS01 pointed out that the disk gas of the primary galaxy is significantly compressed in the early phase of ram pressure stripping. The mechanism of the compression is as follows: initially the disk gas is moved slightly in the direction of the ICM wind, but then the offset gas experiences the gravitational force of the dark-matter halo and tends to fall back to the galactic plane.

¹⁵Active star-formation in the disk of NGC 4388 is indicated not only by bright H α emission but also by many chimney-like structures, which would be formed by supernovae explosions in the disk (cf. Norman and Ikeuchi 1989), seen in the faint level of the emission-line image (see Figure 5 of YOS02).

Its motion is now in the opposite direction to the ICM wind, so that the ICM wind and the gravitational force compress the disk gas from both sides of the disk. This is the situation for a face-on collision, i.e., one in which the galaxy is exposed to the ICM wind face-on. In the case of an inclined collision, the disk gas is also compressed in the disk plane by ram pressure. V CBD have also discussed gas compression of this kind, occurring before prompt stripping. Further, a third process, the gas “annealing” process discussed by SS01, may be efficient in compressing the inner disk. In this process, angular momentum transport by spiral waves induced in the ram pressure stripping event leads to simultaneous expansion of the outer disk and compression of the inner disk. The models of SS01 suggest that by the time the outer disk has been stripped, the inner disk is significantly compressed.

A combination of the above processes must lead to strong compression of the disk gas of NGC 4388. V CBD estimated the compression factor of the gas surface density to be as high as 1.5 for the case of an edge-on collision. Other studies have also suggested that gas compression by a factor of 2 – 3 should occur in the early phases of ram pressure stripping (e.g., Fujita and Nagashima 1999; SS01). This high compression of disk gas should cause active star formation in the disk. Assuming a Schmidt law¹⁶ (Schmidt 1959) with a slope $N \sim 1.5$ (Kennicutt 1998), we find that the star formation rate (SFR) increases by a factor of up to 3 – 5. In fact, the SFR of the NGC 4388 disk, estimated from the H α emission, is $\sim 4 M_{\odot} \text{ yr}^{-1}$, which is consistent with the above value if we assume that the SFR was $\sim 1 M_{\odot} \text{ yr}^{-1}$ before collision with the ICM.

5.4. Global Structure and Evolution of the Emission-line Region of NGC 4388

Finally, we discuss the global structure of the extra-planar emission-line region around NGC 4388. The following emission-line regions are found in and around NGC 4388: (1) disk H II regions, (2) the NE plume and the SW cone (see Figure 2 of YOS02), (3) faint extra-planar spurs (Figure 11d), and (4) the VEELR. Here, we pro-

¹⁶ $\Sigma_{SFR} = A \times \Sigma_{gas}^N$, where Σ_{SFR} is the star formation rate per unit area and Σ_{gas} is the gas surface density.

pose an evolutionary scenario in which the above emission-line regions can be related to each other.

In this scenario we assume that the prime mover of the evolution of the interstellar medium (ISM) of NGC 4388 is the fast collision between the galaxy and the hot ICM of the Virgo cluster. Initially, NGC 4388 was captured by the Virgo cluster during the cluster’s mass assembly process and started to fall into the central region of the cluster. Once the galaxy began to experience ram pressure from the cluster ICM, the ram pressure (and the opposing gravitational force) compressed the disk gas. This would have taken place $\sim 10^7$ yr before the galaxy reached the central region of the cluster. This gas compression caused a starburst in the disk. Successive bursts of supernovae and stellar winds from clusters of young massive stars heated the ISM, causing it to expand into intra-cluster space: i.e., a starburst superwind was formed.

At the same time, the outer disk gas of NGC 4388 began to be stripped by ram pressure. When the galaxy had passed through the cluster center, the ram pressure gradually started to decline and the stripped gas rotated slowly in the rotation direction of the host galaxy as a result of its angular momentum. NGC 4388 probably collided with the ICM to the southwestern side of the disk. As the disk rotation and the ram pressure stripping force had the same direction on the western side of NGC 4388, the western disk gas was the first to be dragged out of the galaxy.

At the eastern side of the disk, where the directions of the disk rotation and the ram pressure force were opposite to each other, the disk gas lost its angular momentum due to deceleration by the ram pressure. This disk gas thus started to fall in toward the nucleus. In fact, this gas infall might have excited the nuclear activity, although the triggering mechanism of AGN is not known in detail and this is just one of several possible hypotheses. Recently, minor merger events have been proposed as a promising mechanism for triggering AGN activity (Taniguchi 1999; Kendall, Magorrian & Pringle 2003). As pointed out in YOS02, the disk of NGC 4388 bears the marks of a past minor merger. Hence, a minor merger might have occurred and triggered the AGN at about the same time that NGC 4388 passed near the cluster center.

To the northeast of the galaxy, the stripped

gas formed an elongated filamentary structure as a result of the combination of its rotation and the ram pressure forces it experienced. According to VCBD, the stripped gas forms highly elongated structures like the VEELR $\sim 10^8$ yr after the time when the ram pressure force reaches its maximum. Therefore, NGC 4388 passed through the cluster central region $\sim 10^8$ yr ago and is now receding from the center of the Virgo cluster.

The interaction between the stripped gas and the starburst superwind accelerated the gas and changed the energy spectrum of the radio-emitting plasma. The radio jet from the AGN of NGC 4388 was possibly accompanied by a warm gas outflow, and Veilleux et al. (1999a) suggested that this outflow might have formed the NE plume. However, we do not believe that the AGN outflow was the primary factor in forming the NE plume, because (1) there is a large discrepancy between the PA of the radio jet and that of the NE plume, (2) the NE plume has a highly disturbed morphology compared to the winds seen in other AGN wind cases, and (3) the velocity of the NE plume is comparable to that of the NE-HV filaments. In addition, the morphology of the NE plume resembles that of the NE-HV filaments. Therefore, we conclude that most of the structure of the NE plume was formed by ram pressure stripping (cf. Corbin, Baldwin & Wilson 1988; Petitjean & Durret 1993). The AGN outflow possibly contributed to the formation of the NE plume, but if so its contribution must have been small.

In the above scenario, the primary cause of the various phenomena occurring in NGC 4388 is the fast collision of the galaxy with the hot ICM. We summarize the structure of the emission-line regions around NGC 4388 as a schematic drawing in Figure 12. The various phenomena in NGC 4388 — the AGN, the starburst, and the ram pressure stripping — will last for only a comparatively short time. After another several tens of millions of years, these activities will cease or decay significantly. As the velocities of many VEELR filaments exceed the escape velocity of NGC 4388, most of the gas in the VEELR will escape into intracluster space. On the other hand, the gas that is presently in the galaxy disk will remain there, because the ram pressure force acting on it will decay. Therefore, NGC 4388 will be observed as an ‘anemic’ spiral galaxy with no peculiar activity

several tens of millions of years from now.

6. Summary

Using the Subaru telescope, we carried out deep optical spectroscopic observations of the very extended emission-line region (VEELR) found around the Seyfert 2 galaxy NGC 4388 in the Virgo cluster. The H α recession velocities of most of the filaments in the VEELR are highly blue-shifted relative to the systemic velocity of the galaxy. The velocity field is complicated and the range of velocities is considerably broad (~ 700 km s $^{-1}$). There are a number of kinematically and morphologically distinct groups of filaments. We classified the filaments into the following groups: the low velocity (“LV”) filaments, the high velocity (“HV”) filaments, and the very high velocity (“VHV”) clouds. The HV filaments consist of the following spatially separated subgroups: the N-HV filaments, the NE-HV filaments, and the W-HV filaments. The emission-line ratios of the VEELR filaments are well explained by power-law photoionization models with solar abundances, suggesting that the Seyfert nucleus of NGC 4388 is the dominant ionization source of the VEELR and that the VEELR gas has moderate metallicity. Shock heating also contributes to the ionization of some filaments. In particular, the western part of the HV filaments (the “W-HV filaments”) may be excited predominantly by shocks.

We conclude that the VEELR was formerly the disk gas of NGC 4388, which has been stripped from the disk by the ram pressure caused by the interaction between the hot intra-cluster medium (ICM) and the galaxy. The velocity field and the morphology of the VEELR closely resemble snapshots taken from some numerical simulations of this situation. In the case of NGC 4388, the ram pressure-stripped gas, which would ordinarily be seen as extended H I filaments, happens to be exposed and ionized by the AGN light, and so can be seen as optical emission-line gas. This special situation makes it possible to study in detail environmental effects, especially ram pressure stripping by the hot ICM, on the evolution of cluster galaxies and intracluster medium.

Finally, we point out that filamentary/clumpy structure of the VEELR suggests that ram pressure-stripped gas may be cooled radiatively and be con-

densed to dense, small clouds as being extended into the inter-galactic space. In other words, most of the debris of ram pressure-stripping could be found as an ensemble of small H I filaments, if the filaments are not ionized by some energetic source like AGNs. Thus high spatial resolution, deep H I survey may be important to make statistics of the ram pressure-stripping phenomena and its impact to the galaxy evolution.

We are grateful to the staff of the Subaru telescope for their kind help with the observations. We wish to thank Curt Struck for his useful comments and the referee for a constructive report. In addition, M. Y. thanks the staff of Okayama Astrophysical Observatory for their encouragement during the course of this work. This study was carried out using the facilities at the Astronomical Data Analysis Center, National Astronomical Observatory of Japan. This research made use of NASA’s Astrophysics Data System Abstract Service. This work was financially supported in part by the Japan Society for the Promotion of Science (Grant-in-Aid for Scientific Research No. 14204018).

REFERENCES

- Abadi, M. G., Moore, B., & Bower, R. G. 1999, *MNRAS*, 308, 947
- Abraham et al. 1996, *ApJ*, 471, 694
- Armus, L., Heckman, T. M., Weaver, K. A., & Lehnert, M. D. 1995, *ApJ*, 445, 666
- Bekki, K., Couch, W. J., & Shioya, Y. 2002, *ApJ*, 577, 651
- Bureau, M., & Carignan, C. 2002, *AJ*, 123, 1316
- Butcher, H., & Oemler, A. 1978, *ApJ*, 219, 18
- Butcher, H., & Oemler, A. 1984, *ApJ*, 285, 426
- Cayatte, V., van Gorkom, J. H., Balkowski, C., & Kotanyi, C. 1990, *AJ*, 100, 604
- Chevalier, R., & Clegg, A. 1985, *Nature*, 317, 44
- Ciroti, S., Contini, M., Rafanelli, P., & Ritcher, G. M., 2003, *A&A*, 400, 859
- Colbert, E. J. M., Baum, S. A., O’Dea, C. P., & Veilleux, S. 1998, *ApJ*, 496, 786
- Colina, L. 1992, *ApJ*, 386, 59

- Corbin, M. R., Baldwin, J. A., & Wilson, A. S. 1988, *ApJ*, 334, 584
- Couch, W. J., Barger, A. J., Smail, I., Ellis, R. S., & Sharples, R. M. 1998, *ApJ*, 497, 188
- Dopita, M. A., & Sutherland, R. A. 1995, *ApJ*, 455, 468
- Dressler, A. 1980, *ApJ*, 236, 351
- Dressler, A. 1994, *ApJ*, 430, 107
- Dressler, A. et al. 1997, *ApJ*, 490, 577
- Falcke, H., Wilson, A. S., & Simpson, C. 1998, *ApJ*, 502, 199
- Fasano, G., Poggianti, B. M., Couch, W. J., Bettori, D., Kjærgaard, P., & Moles, M. 2000, *ApJ*, 542, 673
- Ferland, G. J. 1996, *Hazy, a Brief Introduction to Cloudy*, University of Kentucky Department of Physics and Astronomy Internal Report.
- Fujita, Y., & Nagashima, M. 1999, *ApJ*, 516, 619
- Gavazzi, G., Contursi, A., Carrasco, L., Boselli, A., Kennicutt, R., Scodreggio, M., & Jaffe, W. 1995, *A&A*, 304, 325
- Gavazzi, G., Boselli, A., Mayer, L., Iglesias-Paramo, J., Vilchez, J. M., & Carrasco, L. 2001, *ApJ*, 563, L23
- Gerhard, O., Arnaboldi, M., Freeman, K. C., & Okamura, S. 2002, *ApJ*, 580, L121
- Heckman, T. M., Armus, L., & Miley G. K. 1990, *ApJS*, 74, 833
- Hernquist, L., & Mihos, J. C. 1995, *ApJ*, 448, 41
- Hibbard, J. E., Guhathankurta, P., van Gorkom, J. H., & Schweizer, F. 1994, *AJ*, 107, 67
- Hibbard, J. E., & Yun, M. S. 1999, *AJ*, 118, 162
- Iizuka, T., Kunieda, H., & Maeda, Y. 2003, in *Proceedings of Workshop on Galaxies and Clusters of Galaxies*, ed. T. Ohashi & N. Y. Yamasaki, p29
- Irwin, J. A., English, J., & Sorathis, B. 1999, *AJ*, 117, 2102
- Kaifu, N., et al. 2000, *PASJ*, 52, 1
- Kauffman, G., & Charlot, S. 1998, *MNRAS*, 294, 705
- Kashikawa, N., et al. 2002, *PASJ*, 54, 819
- Kendall, P., Magorrian, J., & Pringle, J. E. 2003, *MNRAS*, accepted.
- Kennicutt, R. C. Jr. 1998, *ARA&A*, 36, 189
- Kenny, J. D. P., & Koopmann, R. A. 1999, *AJ*, 117, 181
- Larson, R. B., Tinsley, B. M., & Caldwell, C. N. 1980, *ApJ*, 237, 692
- Mathewson, D. S., Cleary, M. N., & Murray, J. D. 1974, *ApJ*, 190, 291
- Melnick, J., & Sargent, W. L. W. 1977, *ApJ*, 215, 401
- Mihos, J. C., Walker, I. R., Hernquist, L., Mendes de Oliveira, C., & Bolte, M. 1995, *ApJ*, 447, L87
- Moore, B., Katz, N., Lake, G., Dressler, A., & Oemler, A. 1996, *Nature*, 379, 613
- Moore, B., Lake, G., & Katz, N. 1998, *ApJ*, 495, 139
- Norman, C. A., & Ikeuchi, S. 1989, *ApJ*, 345, 372
- Okamoto, T., & Nagashima, M. 2001, *ApJ*, 547, 109
- Osterbrock, D. E., 1989, *Astrophysics of Gaseous Nebulae and Active Galactic Nuclei* (University Science Books)
- Oemler, A. 1974, *ApJ*, 194, 1
- Oemler, A., Dressler, A., & Butcher, H. 1997, *ApJ*, 474, 561
- Petitjean, P., & Durret, F. 1993, *A&A*, 277, 365
- Phookun, B., & Mundy, L. G. 1995, *ApJ*, 453, 154
- Pogge, R. W. 1988, *ApJ*, 332, 702
- Poggianti, B. M. et al. 1999, *ApJ*, 518, 576
- Postman, M., & Geller, M. J. 1984, *ApJ*, 281, 95
- Quilis, V., Moore, B., & Bower, R. 2000, *Science*, 288, 1617
- Robinson, A. et al. 1994, *A&A*, 291, 351
- Ryder, S. D., Purcell, G., Davis, D., & Andersen, V. 1997, *PASA*, 14, 1
- Schmidt, M. 1959, *ApJ*, 129, 243
- Schulz, S., & Struck, C. 2001, *MNRAS*, 328, 185 (SS01)
- Smith, B. J. 1994, *AJ*, 107, 1695
- Strickland, D. K., & Stevens, I. R. 2000, *MNRAS*, 314, 511
- Taniguchi, Y. 1999, *ApJ*, 524, 65

- Veilleux, S., & Osterbrock, D. M. 1987, ApJS, 63, 295
- Veilleux, S., Bland-Hawthorn, J., Cecil, G., Tully, B., & Miller, S. T. 1999a, ApJ, 520, 111
- Veilleux, S., Bland-Hawthorn, J., & Cecil, G., 1999b, AJ, 118, 2108
- Vílchez, J. M., & Iglesias-Páramo, J. 2003, ApJS, 145, 225
- Vollmer, B., Marcelin, M., Amram, P., Balkowski, C., Cayatte, V., & Garrido, O. 2000, A&A, 364, 532
- Vollmer, B., Cayatte, C., Balkowski, C., & Duschl, W. J. 2001, ApJ, 561, 708 (VCBD)
- Vollmer, B., Braine, J., Balkowski, C., Cayatte, V., & Duschl, W. J. 2001, A&A, 374, 824
- Walker, I. R., Mihos, J. C., & Hernquist, L., 1996, ApJ, 460, 121
- Webb, G. M., Ko, C. M., Zank, G. P., & Jokipih, J. R. 2003, ApJ, 595, 193
- Yasuda, N., Fukugita, M., & Okamura, S. 1997, ApJS, 108, 417
- Yoshida, M. et al. 2000, Proc. of SPIE, 4009, 240
- Yoshida, M. et al. 2002, ApJ, 567, 118 (YOS02)

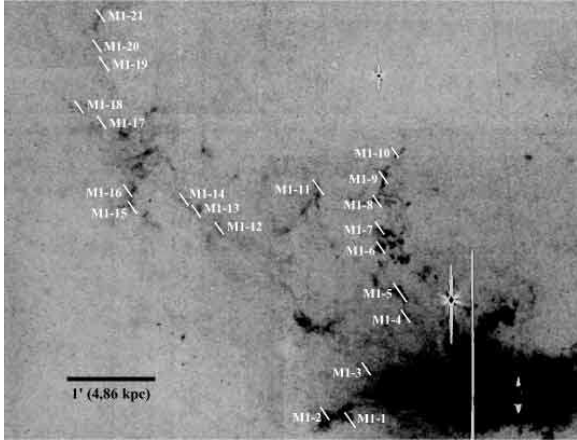


Fig. 1.— Figures 1 and 2 show the layouts of the slits. This figure shows the slit layout of MOS mask 1. The width of each slit is $0''.8$ on the sky. The scale bar indicates $1'$.

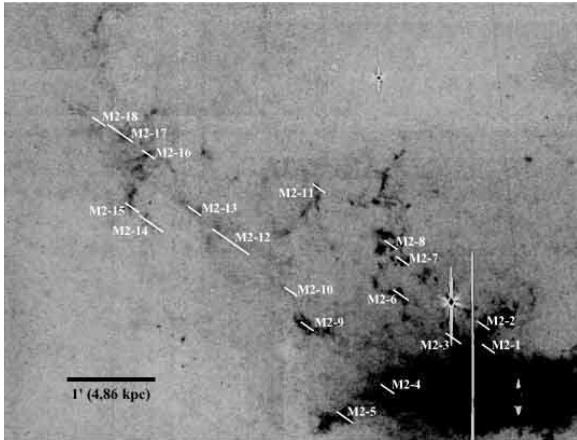


Fig. 2.— The slit layout of the MOS mask 2.

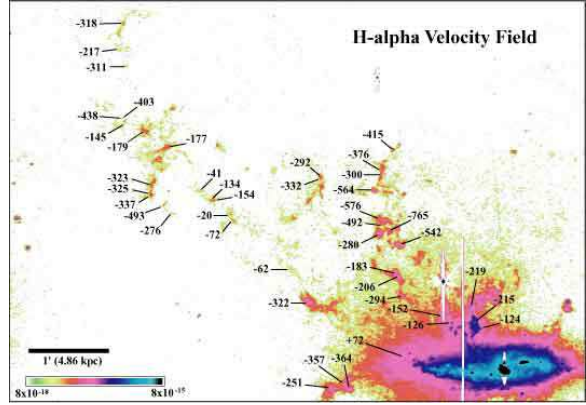


Fig. 3.— The velocity field of the VEELR of NGC 4388 overplotted on the $H\alpha + [N II]$ image of YOS02. The scale-bar at the left-bottom corner shows logarithmic scale of the surface brightness of the $H\alpha$ emission in units of $\text{erg s}^{-1} \text{cm}^{-2} \text{arcsec}^{-2}$. Radial velocities relative to the systemic velocity of the galaxy (2525 km s^{-1}) are shown. Note that almost all the filaments measured are blue-shifted relative to the galaxy. The velocity field is complicated and there are significant velocity jumps in some regions.

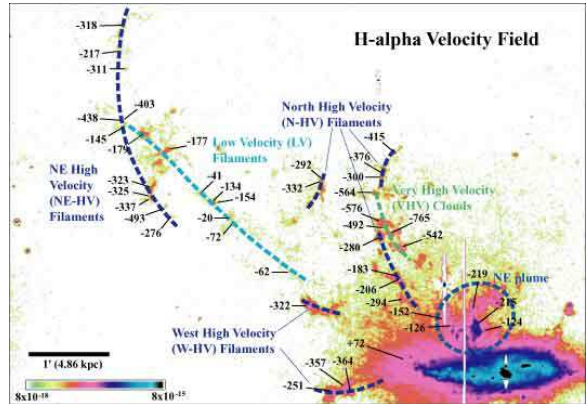


Fig. 4.— Schematic lines indicating individual groups of filaments/clouds suggested by their morphological and kinematical characteristics (see the text) are overlaid on the velocity field of the VEELR.

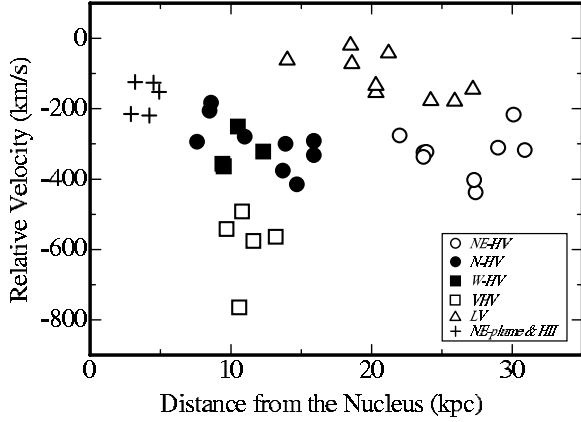


Fig. 5.— Distance - velocity diagram for the VEELR. Different symbols indicate different groups of filaments/clouds as follows: open circles, the NE-HV filaments; filled circles, the N-HV filaments; filled squares, the W-HV filaments; open squares, the VHV clouds; triangles, the LV filaments; and crosses, the NE-plume and parts of the disk H II regions.

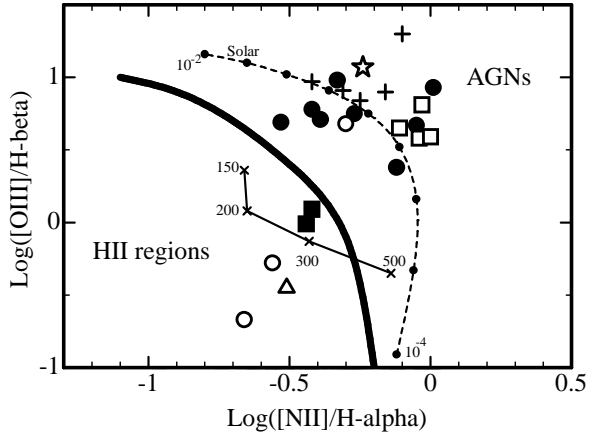


Fig. 7.— Fig.7 - Fig.9 show emission-line diagnostic diagrams for the VEELR filaments. Each axis of the diagrams has a logarithmic scale. The symbols used in the diagrams are the same as in Figure 5. A star symbol indicates data from the nuclear spectrum taken by Colina (1992). This figure shows the $[O III]\lambda 5007/H\beta$ ratio vs. the $[N II]\lambda 6584/H\alpha$ ratio. The thick solid lines in the diagrams indicate the boundary between AGN-like spectra and H II region-like spectra. The dashed lines are loci of a power-law photoionization model calculated using CLOUDY (Ferland 1996). The electron density and the spectral index α of the incident continuum of the model are 30 cm^{-3} and -1.4 , respectively. The metal abundance of the model is the solar value. The filled circles on the loci represent a series of ionization parameters U , from $U = 10^{-4}$ to $U = 10^{-2}$, with intervals of $\log U = 0.25$. The thin-solid lines are loci of the radiative shock model (a “shock only” model with no magnetic field) of Dopita and Sutherland (1995). The crosses on the loci indicate the shock velocity, ranging from 150 km s^{-1} to 500 km s^{-1} .

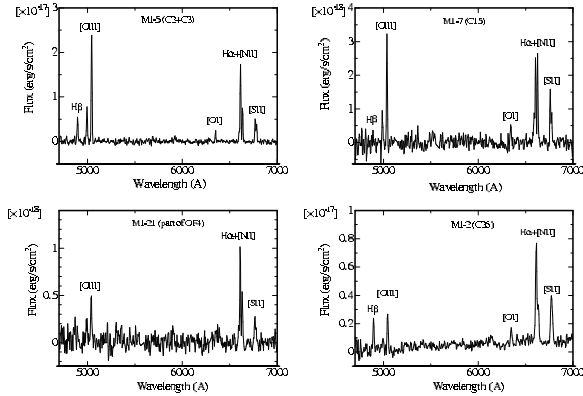


Fig. 6.— Some examples of spectra of filaments of the VEELR. Top left: the spectrum of filaments C2 and C3 (YOS02) through slit M1-5. Top right: the spectrum of filament C15 through slit M1-7. Bottom left: the spectrum of the most distant filament measured in this study. This spectrum was taken through slit M1-21. Bottom right: the spectrum of filament C26 through slit M1-2.

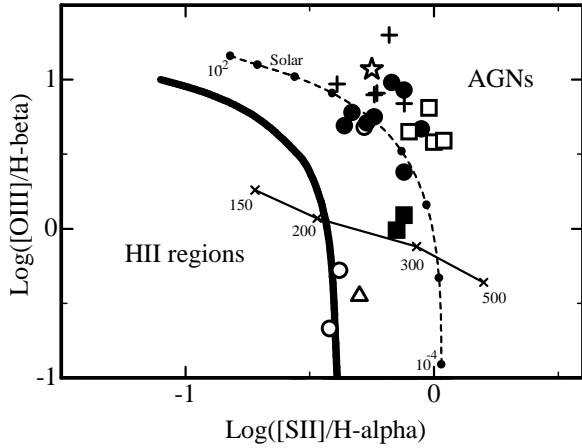


Fig. 8.— [O III] $\lambda 5007/H\beta$ ratio vs. [S II] $\lambda 6716+\lambda 6731/H\alpha$ ratio diagram. The meanings of the symbols and lines are the same as in Figure 7.

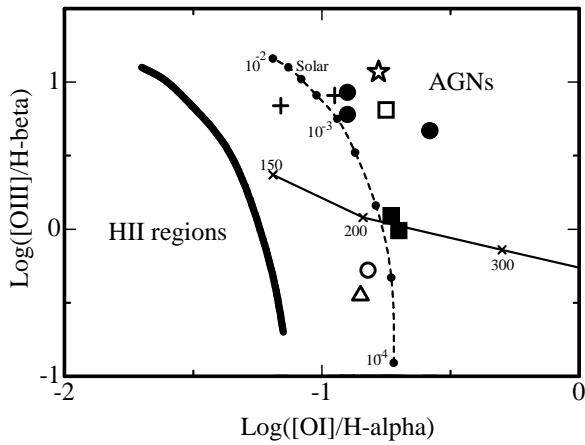


Fig. 9.— [O III] $\lambda 5007/H\beta$ ratio vs. [O I] $\lambda 6300/H\alpha$ ratio diagram. The meanings of the symbols and lines are the same as in Figure 7.

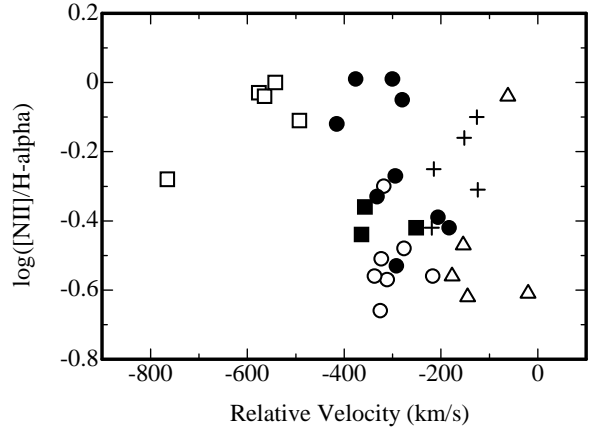


Fig. 10.— Velocity – emission line intensity ratio ($\log([N II]/[H\alpha])$) diagram. The meanings of the symbols are the same as in Figure 5.

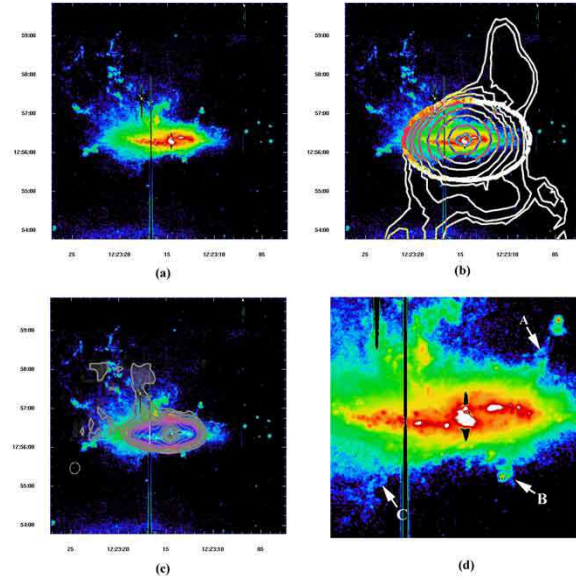


Fig. 11.— Comparison between the VEELR and the radio plasma distribution taken by Irwin et al. (1999). a) The $H\alpha$ image (YOS02). b) The 20 cm image overlaid on the $H\alpha$ image. c) The 6 cm image overlaid on the $H\alpha$ image. d) An expanded $H\alpha$ image of the central region of NGC 4388. Three faint spurs (“A”, “B” and “C”) are indicated by arrows.

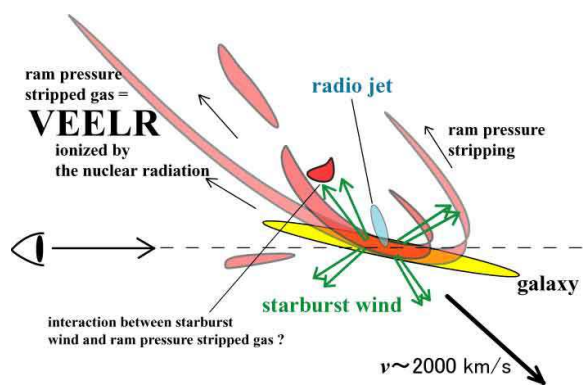


Fig. 12.— Schematic draw of the structure of the emission-line regions around NGC 4388.

TABLE 1
PHYSICAL PARAMETERS OF THE VEELR GAS CLOUDS

Slit ID	distance ^a	length ^b	$f_{\text{H}\alpha}$ ^c	$V_{\text{H}\alpha}$ ^d	$FWHM$ ^e	Cloud ID ^f	Group ^g
M1-1	9.5	150	14.6	-364 ±19	200	C26	W-HV
M1-2	10.5	160	11.1	-251 ±20	530	C26	W-HV
M1-4	7.6	230	3.3	-294 ±22	180	C1	N-HV
M1-5	8.6	450	21.1	-183 ±19	...	C2+C3	N-HV
M1-6	11.0	310	6.6	-280 ±20	...	C11	N-HV
M1-7	11.6	190	3.6	-576 ±21	...	C15	VHV
M1-8	13.2	260	4.6	-564 ±20	...	C16	VHV
M1-9-1	13.7	50	0.3	-376 ±87	...	C18	N-HV
M1-9-2	13.9	160	2.5	-300 ±20	...	C18	N-HV
M1-10	14.7	150	2.8	-415 ±21	...	C19	N-HV
M1-11	15.9	310	4.9	-292 ±21	80	C22	N-HV
M1-12	18.5	110	0.7	-20 ±32	320	part of OF1	LV
M1-13	20.3	160	1.6	-154 ±22	...	part of OF1	LV
M1-14	21.2	100	0.4	-41 ±47	...	part of OF1	LV
M1-15 ^h	23.7	160	4.1	-325 ±22	280	part of OF2	NE-HV
M1-16 ^h	23.9	150	3.3	-323 ±23	...	part of OF2	NE-HV
M1-17-1	27.2	80	0.6	-145 ±26	...	part of OF2	LV
M1-17-2	27.4	100	0.8	-438 ±71	...	part of OF2	NE-HV
M1-19 ^h	29.0	100	1.0	-311 ±22	...	part of OF4	NE-HV
M1-20	30.1	80	0.3	-217 ±30	...	part of OF4	NE-HV
M1-21	30.9	160	1.3	-318 ±24	...	part of OF4	NE-HV
M2-1-1	2.9	150	21.0	-215 ±19	...	part of NE plume	NEp
M2-1-2	3.2	180	31.7	-124 ±19	30	part of NE plume	NEp
M2-2	4.2	440	15.8	-219 ±20	40	part of NE plume	NEp
M2-3-1	4.5	180	8.0	-126 ±21	140	part of NE plume	NEp
M2-3-2	4.9	80	2.5	-152 ±21	...	part of NE plume	NEp
M2-4	6.1	130	1.4	+72 ±26	...	disk H II region	disk
M2-5	9.4	340	11.5	-357 ±21	...	C26	W-HV
M2-6	8.5	320	14.7	-206 ±20	350	C2+C3	N-HV
M2-7 ⁱ	9.7	190	4.9	-542 ±20	...	C8	VHV
M2-8-1	10.6	100	1.3	-765 ±31	...	C12	VHV
M2-8-2	10.8	100	2.5	-492 ±23	140	C12	VHV
M2-9 ^j	12.3	60	0.9	-322 ±132	460	C25	W-HV
M2-10 ^h	14.0	80	0.6	-62 ±30	...	part of OF1	LV
M2-11	15.9	230	4.3	-322 ±24	230	C22	N-HV
M2-12	18.6	230	2.0	-72 ±31	70	part of OF1	LV
M2-13	20.3	80	0.7	-134 ±25	...	part of OF1	LV
M2-14-1	22.0	130	1.1	-276 ±33	250	part of OF2	NE-HV
M2-14-2	22.7	340	2.7	-493 ±32	...	part of OF2	NE-HV
M2-15	23.7	160	4.4	-337 ±20	200	part of OF2	NE-HV
M2-16	24.2	160	3.4	-177 ±21	290	part of OF2	LV
M2-17	25.9	360	9.2	-179 ±21	280	part of OF2	LV
M2-18	27.3	190	1.2	-403 ±30	...	part of OF2	NE-HV

^adistance from the nucleus in units of kpc.

^bintegration length along slit in units of pc.

^cH α flux in units of 10^{-17} erg s $^{-1}$ cm $^{-2}$.

^dvelocity relative to the systemic velocity of NGC 4388 (2525 km s $^{-1}$): km s $^{-1}$.

^efull width at half maximum of the H α lines in units of km s $^{-1}$.

^fThe cloud identification of YOS02.

^gThe kinematical and morphological group identification defined in this work (see the text)

^hCCD defect near [O III] λ 5007.

ⁱCCD defect pattern at the edge of the slit.

^jCCD defect pattern pollutes half of the spectrum along the slit.

TABLE 2
EMISSION-LINE INTENSITY RATIOS OF THE VEELR GAS CLOUDS

Slit ID	Log([O III]/H β)	Log([N II]/H α)	Log([S II]/H α)	Log([O I]/H α)
M1-1	-0.01 \pm 0.11	-0.44 \pm 0.06	-0.15 \pm 0.06	-0.70 \pm 0.10
M1-2	0.09 \pm 0.10	-0.42 \pm 0.06	-0.12 \pm 0.06	-0.73 \pm 0.10
M1-4	0.75 \pm 0.08	-0.27 \pm 0.06	-0.24 \pm 0.06	...
M1-5	0.78 \pm 0.08	-0.42 \pm 0.06	-0.33 \pm 0.06	-0.90 \pm 0.10
M1-6	0.67 \pm 0.08	-0.05 \pm 0.06	-0.05 \pm 0.06	-0.58 \pm 0.10
M1-7	0.81 \pm 0.09	-0.03 \pm 0.06	-0.02 \pm 0.06	-0.75 \pm 0.11
M1-8	0.58 \pm 0.08	-0.04 \pm 0.06	0.00 \pm 0.06	...
M1-9-1	...	0.01 \pm 0.07	-0.14 \pm 0.08	...
M1-9-2	0.93 \pm 0.09	0.01 \pm 0.06	-0.12 \pm 0.06	-0.90 \pm 0.11
M1-10	0.38 \pm 0.09	-0.12 \pm 0.06	-0.12 \pm 0.06	...
M1-11	0.69 \pm 0.09	-0.53 \pm 0.06	-0.36 \pm 0.06	...
M1-12	...	-0.61 \pm 0.08
M1-13	...	-0.47 \pm 0.06	-0.25 \pm 0.06	...
M1-14
M1-15	...	-0.66 \pm 0.06	-0.42 \pm 0.06	...
M1-16	...	-0.51 \pm 0.06	-0.26 \pm 0.06	...
M1-17-1	...	-0.62 \pm 0.07	-0.09 \pm 0.06	...
M1-17-2	-0.37 \pm 0.07	...
M1-19	...	-0.57 \pm 0.06	-0.30 \pm 0.06	...
M1-20	...	-0.56 \pm 0.08
M1-21	0.68 \pm 0.11	-0.30 \pm 0.06	-0.28 \pm 0.06	...
M2-1-1	0.84 \pm 0.08	-0.25 \pm 0.06	-0.12 \pm 0.06	-1.16 \pm 0.11
M2-1-2	0.91 \pm 0.08	-0.31 \pm 0.06	-0.23 \pm 0.06	-0.95 \pm 0.10
M2-2	0.97 \pm 0.08	-0.42 \pm 0.06	-0.39 \pm 0.06	...
M2-3-1	1.30 \pm 0.09	-0.10 \pm 0.06	-0.18 \pm 0.06	...
M2-3-2	0.90 \pm 0.08	-0.16 \pm 0.06	-0.24 \pm 0.06	...
M2-4	-0.55 \pm 0.08	...
M2-5	...	-0.36 \pm 0.06	-0.23 \pm 0.06	...
M2-6	0.71 \pm 0.08	-0.39 \pm 0.06	-0.27 \pm 0.06	...
M2-7	0.59 \pm 0.08	0.00 \pm 0.06	0.04 \pm 0.06	...
M2-8-1	...	-0.28 \pm 0.06	-0.14 \pm 0.06	...
M2-8-2	0.65 \pm 0.09	-0.11 \pm 0.06	-0.10 \pm 0.06	...
M2-9	...	-0.15 \pm 0.07
M2-10
M2-11	0.98 \pm 0.12	-0.33 \pm 0.06	-0.17 \pm 0.06	...
M2-12	...	-0.74 \pm 0.09	-0.25 \pm 0.06	...
M2-13	...	-0.96 \pm 0.10	-0.24 \pm 0.06	...
M2-14-1	...	-0.48 \pm 0.07	-0.37 \pm 0.07	...
M2-14-2	...	-0.63 \pm 0.08	-0.35 \pm 0.06	...
M2-15	-0.28 \pm 0.16	-0.56 \pm 0.06	-0.38 \pm 0.06	-0.82 \pm 0.11
M2-16	...	-0.56 \pm 0.06	-0.29 \pm 0.06	...
M2-17	-0.45 \pm 0.21	-0.51 \pm 0.06	-0.30 \pm 0.06	-0.85 \pm 0.11
M2-18	0.02 \pm 0.06	...